This document is the accepted manuscript version of the following article:
Marelli, E., Gazquez, J., Poghosyan, E., Müller, E., Gawryluk, D. J., Pomjakushina, E., … Fabbri, E. (2021).
Correlation between oxygen vacancies and oxygen evolution reaction activity for a model electrode: PrBaCo2O5+δ.
Angewandte Chemie International Edition. https://doi.org/10.1002/anie.202103151
WILEY-VCH

RESEARCH ARTICLE

Correlation between Oxygen Vacancies and Oxygen Evolution Reaction Activity for a Model Electrode: $PrBaCo_2O_{5+\delta}$

Elena Marelli, [a] Jaume Gazquez, [b] Emiliya Poghosyan, [a] Elisabeth Müller,[a] Dariusz J. Gawryluk,[a] Ekaterina Pomjakushina,[a] Denis Sheptyakov,[a] Cinthia Piamonteze,[a] Dino Aegerter, [a] Thomas J. Schmidt, [a,c] Marisa Medarde, [a]* and Emiliana Fabbri*[a]

[a] Dr. E. Marelli, Dr. E. Poghosyan, Dr. E. Müller, Dr. D. J. Gawryluk, Dr. E. Pomjakushina, Dr. D Sheptyakov, Dr. C. Piamonteze, D. Aegerter, Prof. Dr. T.J. Schmidt, Dr. M. Medarde, Dr. E. Fabbri
Paul Scherrer Institute
Forschungsstrasse 111 5232 Villigen PSI, Switzerland
E-mail: marisa.medarde@psi.ch, emiliana.fabbri@psi.ch
[b] Dr. J, Gazquez
Institut de Ciència de Materials de Barcelona (ICMAB-CSIC)
Campus UAB, Bellaterra 08193, Barcelona, Spain
[c] Prof. T. J. Schmidt
Laboratory of Physical Chemistry, ETH Zurich
8093 Zurich, Switzerland

Supporting information for this article is given via a link at the end of the document.((Please delete this text if not appropriate))

Abstract: The role of the perovskite lattice oxygen in the oxygen evolution reaction (OER) is systematically studied in the $PrBaCo_2O_{5+\delta}$ family. The reduced number of physical/chemical variables combined with in-depth characterizations such as neutron dif-fraction, O K-edge X-ray absorption spectroscopy (XAS), electron energy loss spectroscopy (EELS), magnetization and scanning transmission electron microscopy (STEM) studies, helps investigating the complex correlation between OER activity and a single perovskite property, such as the oxygen content. Larger amount of oxygen vacancies appears to facilitate the OER, possibly contributing to the mechanism involving the oxidation of lattice oxygen, i.e., the lattice oxygen evolution reaction (LOER). Furthermore, not only the number of vacancies but also their local arrangement in the perovskite lattice influences the OER activity, with a clear drop for the more stable, ordered stoichiometry.

Introduction

In the strong and global commitment to reduce the carbon footprint of human activities, the substitution of fossil fuels with green electricity is of fundamental relevance. In particular, hydrogen is considered as the future energy vector. Hydrogen, produced from the surplus of electricity of intermittent renewable resources by water electrolyzers and utilized by fuel cells to locally generate electricity on demand, represents a zero-carbon emission fuel.

In recent years, great efforts have been dedicated to the understanding of the water-splitting mechanism and to the improvement of electrocatalyst materials.[1] In particular, the anodic reaction, the oxygen evolution reaction (OER), is affected by slow kinetics and by significant overpotentials, even with the state-of-the-art electrocatalysts such as IrO_2.[2] The broad commercialization of green-hydrogen technologies urges for the use of highly active, stable and cost-effective electrocatalyst materials. Significant interest and promising results in alkaline environment came from perovskite-type oxides, where the large chemical flexibility allows for a broad variety of elemental compositions and fine properties tuning.[3] Despite the great scientific interest and efforts, however, there is still no univocal consensus on the oxygen evolution reaction mechanism and on the perovskite electrochemical contribution in the OER. In recent years, the involvement of the perovskite lattice oxygen in the oxygen evolution, the so called lattice oxygen evolution reaction (LOER) was theoretically postulated[4] and experimentally proven by few studies.[5] Several mechanisms were proposed for the LOER, most of which involve the participation of the oxygen ions (and not the metals) as active sites for the OH* adsorption and molecular oxygen evolution (for a detailed summary of the different LOER mechanisms we refer to ref. 6). The oxidation of lattice oxygen can lead to the creation of superficial oxygen vacancies; the latter can be then replaced by OH- ions from the electrolyte forming on the perovskite surface an oxyhydroxide layer.[6] Several studies on different perovskite oxides show that a high oxygen vacancy content is often associated with high OER activity and claim that for these perovskite catalysts the oxygen evolution takes place via the LOER mechanism.[7] For the $La_{1-x}Sr_xCoO_{3-d}$ perovskites, Mefford et al.[7d] reported that the higher the covalent character of the Co-O bond the higher the vacancy concentration, and also the OER activity. Also for $La_{0.5}Sr_{1.5}Ni1-_xFe_xO_{4+d}$ Ruddlesden-Popper structures, Si-modified $SrCoO_3$[7e] and a Ruddlesdedn-Popper/perovskite hybrid system ($LaSr_3Co_{1.5}Fe_{0.5}O_{3-d}/La_{0.25}Sr_{0.75}Co_{0.5}Fe_{0.5}O_{3-d}$),[7f] a correlation between lattice oxygen vacancies and OER activity has been revealed.[7c] However, the univocal influence of the lattice oxygen vacancies initially present in the pristine perovskite structure, not only in their content but also in their distribution, on the OER activity is still unclear. In fact, the most common approach in the search of a correlation between oxygen vacancies and OER activity is based on the screening and comparison of perovskites with a different composition (i.e., changing the Sr or the Fe content in the $La_{1-x}Sr_xCoO_{3-d}$ or in the $La_{0.5}Sr_{1.5}Ni1-_xFe_xO_{4+d}$, respectively). However, changing the perovskite composition leads to perovskite structures with significantly different chemical and physical properties (e.g. metal electronegativity and oxidation state, structure and conductivity), making the comparison of one single activity descriptor ineffective, as previously reported by Cheng et al.[8] . Furthermore, in the OER regime different reactions, namely the conventional OER mechanism, the LOER and, the metal dissolution, can simultaneously occur, further complicating the correlation of a single perovskite properties with the OER activity. Indeed, if the tested perovskites have different (electro)chemical stability or a different OER mechanism takes

10.1002/anie.202103151

place on their surface, a correct interpretation of the oxygen-vacancies/OER activity correlation can be challenging.

In this work, we propose a systematic and in-depth study of the impact of lattice oxygen vacancies on the OER activity. The use of only one material, one of the most OER active perovskites, $PrBaCo_2O_{5+\delta}$ (PBCO),[9] helps reducing the number of chemical and physical variables in the system. This double perovskite is known in the literature for its ability to accommodate a broad range of oxygen vacancies,[10] making it the ideal candidate to validate the impact of the lattice oxygen vacancies in the OER activity. Furthermore, the OER activity of PBCO nanopowder was found to linearly scale with the electrolyte pH value in alkaline environment, which is commonly taken as an indicator of the occurrence of the LOER mechanism.[11] For a detailed analysis of the average amount and distribution of oxygen atoms in the bulk PBCO samples, powder neutron diffraction has been used. Despite the same cationic elemental composition is present in all the samples, the different oxygen stoichiometry causes different intrinsic local and average electronic properties, assessed in this work through the Co and O K-edge X-ray absorption spectroscopy (XAS), electron energy loss spectroscopy (EELS), magnetisation and electronic conductivity measurements. Moreover, the total electron (TEY) and total fluorescence yield (TFY) XAS analysis combined with the scanning transmission electron microscopy (STEM) and EELS clearly show the difference between bulk and surface crystal electronic structures, underling the complex scenario behind the choice of the most active OER electrocatalyst.

Results and Discussion

Structural characterisation and O vacancy distribution

Electrochemical studies often focus on the selection of the cationic composition that allows for the highest activity and stability of the perovskite-based electrocatalyst.[3a] Up until few years ago, very little attention was paid on the anionic stoichiometry, which however is of fundamental importance to determine the catalysts properties and in particular its (L)OER activity. It is of common knowledge that perovskite structures can accommodate a broad range of oxygen stoichiometries, depending strongly on the synthesis conditions, without compromising the main structural scaffold, but with significant changes in the physical properties of the materials.[12]

In order to get information about the oxygen content and its distribution in the crystal lattice we employed a combination of X-ray and neutron powder diffraction data (Figure 1 and Figure S1, Supporting Information). The use of this last technique, more sensitive to light elements than X-ray diffraction, was necessary in order to get reliable information on the oxygen positions and occupations. The oxygen content was determined both via neutron diffraction data refinement and iodometric titration. The obtained values are in good agreement and close to the target oxygen stoichiometries, as shown in Table S1 and Table S2, Supporting Information. Due to the intrinsic higher precision of the titration method in single-phase samples[13] (one order of magnitude difference), these values where chosen over the refined results. The PBCO samples are therefore $PrBaCo_2O_{5.802(3)}$, $PrBaCo_2O_{5.702(8)}$, $PrBaCo_2O_{5.615(3)}$, $PrBaCo_2O_{5.483(1)}$ and $PrBaCo_2O_{5.432(4)}$, for simplicity identified throughout the text as δ = 0.8, 0.7, 0.6, 0.48 and 0.43 respectively.

The vacancy-free $PrBaCo_2O_6$ parent crystal structure (δ = 1, space group *P*4/*mmm*) can be described as an infinite network of corner-sharing [CoO_6] octahedral hosting equal amounts of Co^{3+} and Co^{4+}. The A-positions of the ABO_3 perovskite structure are occupied by two different cations (Pr^{3+} and Ba^{2+}), that due to the large difference between their ionic radii, order in layers perpendicular to the *c* crystal axis.[14] The unit cell, with lattice parameters a_c x a_c x ~2a_c (a_c refers to the pseudocubic parent perovskite lattice) contains thus two perovskite units.

On reducing the oxygen content, the resulting oxygen vacancies are accommodated in the Pr^{3+} layers. The coordination geometry of some of the Co atoms decreases thus from octahedral to square-pyramidal (Figure 2). For moderate amounts of O vacancies, such as in the PBCO samples with δ = 0.8 and 0.7, the tetragonal *P*4/*mmm* symmetry of the parent compound is preserved, indicating a homogeneous distribution of the oxygen vacancies and thus of the CoO_6 octahedral and CoO_5 pyramidal sites (Figure 2).

For the samples with larger amounts of O vacancies (δ = 0.6, 0.48 and 0.43), the high-resolution SXRPD data clearly show the presence of an orthorhombic distortion (space group *Pmmm*, highlighted in the inset in Figure 1b). The distortion, reported for several double-perovskite compounds with δ close 0.5 (Figure S2, Supporting Information),[10a, 12] is caused by the ordering of the oxygen vacancies, and is easily identifiable in the SXRPD patterns through the splitting of some Bragg reflections (Figure 1). The crystal structure is characterised by a larger unit cell (a_cx ~2a_c x ~2a_c), and by the presence of two crystallographically

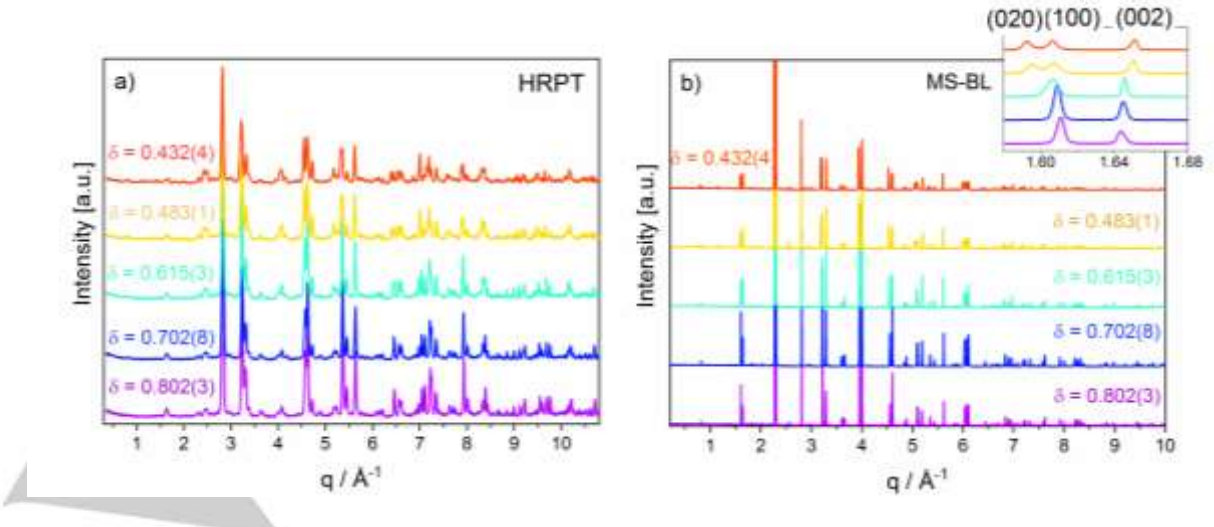

Figure 1. Neutron (a) and synchrotron (b) powder diffraction data of the PBCO samples. The inset in the X-ray data highlights the splitting of the (020) and (100) Bragg reflections as consequence of the orthorhombic distortion present in the samples with O stoichiometry close to δ = 0.5.

independent Co sites (octahedral and square pyramidal) (Figure 2). In an ideal, perfectly ordered composition with δ = 0.5, the alternation of octahedral and pyramids forms oxygen vacancy channels along the *b* direction. Further details on the refined crystal structures are listed in Table S1 and Table S2, Supporting Information.

The decrease of the average Co coordination and the resulting decrease of the nominal Co oxidation state (nominally Co^{4+} in $PrBaCo_2O_6$) has an important impact in the evolution of the average Co-O distance $<d_{Co-O}>$. As shown in Figure S3a (Supporting Information), $<d_{Co-O}>$ grows continuously with increasing number of O vacancies. This is consistent with the increase of the average Co ionic radius <r>, as expected by introducing Co in lower oxidation states ($<r_{Co2+}>$ = 0.69 Å, $<r_{Co3+}>$ = 0.58 Å, $<r_{Co4+}>$ = 0.53 Å, average values considering all the possible spin states),[15] a trend confirmed by X-ray spectroscopies as detailed later in the text. We also observe an increase of the in-plane average O-Co-O buckling angle <θ> (Figure S3b, Supporting Information). This observation is most probably related to the need of accommodating two different Co coordination polyhedra in the structure (octahedra and square pyramid), and to their tendency to order when approaching δ = 0.5. We note that the increase of <θ> involves a less efficient overlap between the O 2p and Co 3d orbitals, suggesting a progressive reduction of the bandwidth[16] (and hence the electronic conductivity) in our samples by increasing the number of O vacancies (Figure S3, Supporting Information).[17] As we will show later, this trend is also confirmed by impedance spectroscopy measurements.

Beyond the oxygen stoichiometry: the electronic configuration

The different oxygen stoichiometries in the PBCO samples have important consequences in the (nominal) cobalt average oxidation state[18] (as shown by the progressive decrease of the average Co oxidation state shown in the Co K-edge XANES spectra in Figure S4, Supporting Information), which results from a combination of Co^{2+} and Co^{3+} for δ < 0.5 and of Co^{3+} and Co^{4+} for δ > 0.5. It has been shown that the Co oxidation state in the pristine perovskite electrocatalyst, such as $Ba_{0.5}Sr_{0.5}Co_{1-x}Fe_xO_{3-\delta}$, $La_{0.2}Sr_{0.8}Co_{1-x}Fe_xO_{3-\delta}$ and PBCO,[5a, 7b, 19] strongly impacts the OER activity. The Co oxidation state has an influence not only on the local geometry, as detailed in the previous section, but also on the electronic configuration of the cobalt atoms. The evolution of the spectra pre-edges are associated to the *1s* --> *3d* transition and can thus provide direct information on the evolution of the density of the empty Co *3d* states.[20] Unfortunately, the extremely complex cobalt environment (2 Co atoms in 2 geometries, 2 oxidation states and 3 possible spin configurations each) prevents the resolution of the different crystal electric field (CEF) splittings in the Co K pre-edge XANES data (Figure S4). In fact, the octahedral CEFs split the *3d* levels into a triplet t_{2g} and a doublet e_g, and these levels are further split when the Co coordination is reduced to square-pyramidal (see Figure 4). An additional difficulty comes from the Δ_{CEF} and the intra-atomic Hund repulsion (J_H) similarity in cobalt. As a consequence, Co compounds are prone to display temperature-dependent *3d* orbital occupations. The close proximity of the Co L2 and L3 edges to the Ba M4 and M5 absorption edges (Figure S4, supporting information), invalidate the use of these spectra as further confirmation of the Co electronic configuration.

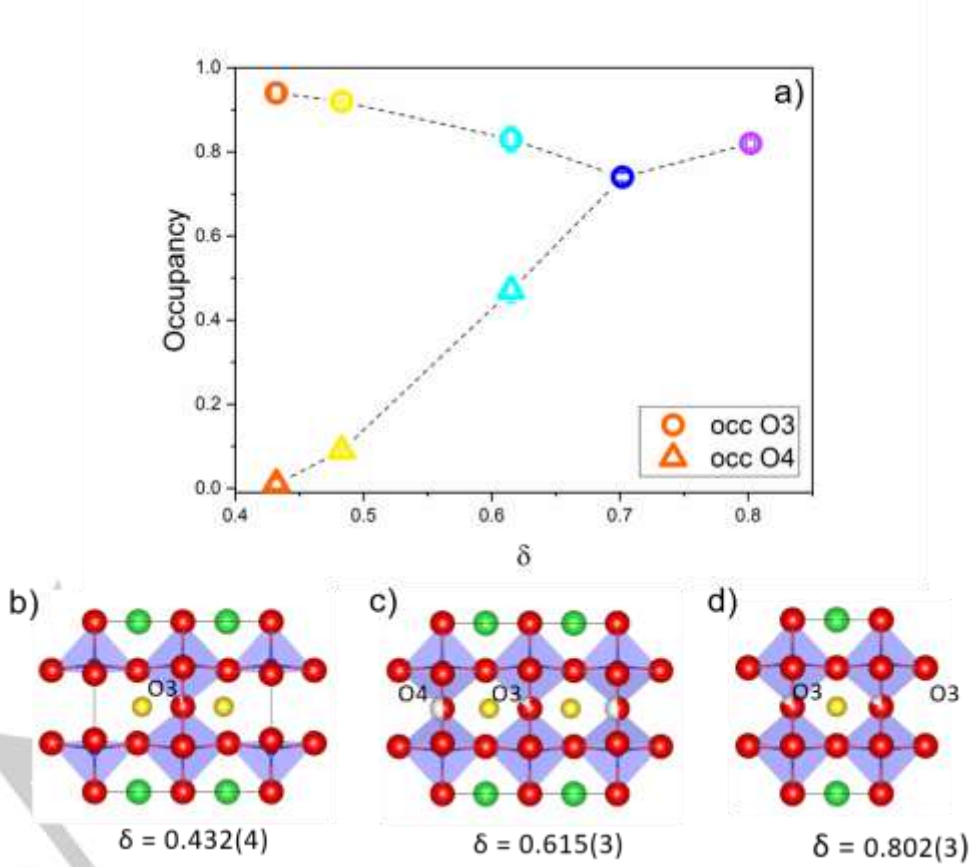

Figure 2. Crystal structure of three representative members of the PBCO family (δ = 0.43 (b), 0.6 (c) and 0.8 (d)) depicted along the *a* direction. Legend: Ba atoms in green, Pr in yellow, Co in blue and O in red. The occupancy distribution of the oxygen atoms in the Pr layer (O3 and O4 in the schemes) of the five samples is reported in (a).

Insights into the PBCO electronic structure came from the O K-edge XAS spectra (Figure 3), where the TFY and TEY detection modes additionally allowed for the simultaneous observation of the bulk (50 - 100 nm) and surface (2 - 5 nm) characteristic absorption edges. Therefore, comparison of TEY and TFY data allows for a depth-profile analysis of the PBCO particles. As showed in Figure 3, the TEY and the TFY spectra are substantially different for *all* samples, especially when considering the pre-edge region (see Figure S5 for details). Given the different thicknesses probed by both techniques these results suggest a reconstruction of the PBCO crystal structure close to the particles surface with important consequences for the Co 3d electronic structure.

The pre-edge region of the O K-edge XAS spectra (Figure 3 and Figure S5, Supporting Information) is normally associated to the transitions from the O *1s* to the O *2p* orbitals overlapping with the Co *3d* bands. In a first order approximation, the area between ≈ 527 and 531 eV can thus be seen as a projection of the total density of unoccupied Co *3d* states.

The role of the metal electronic configuration in the perovskite electrocatalysts OER activity has been widely debated.[2a, 3, 8, 21] The e_g orbital filling of 1 electron has been proposed as perovskite OER activity descriptor, though this conclusions are based on average and theoretical orbital occupancies, not necessarily verified by accurate spin-state determinations, nor to specific compositions (*e.g.* oxygen stoichiometry).[2a, 3, 21c] The O pre-edge XANES peaks intensities can give insights to the electronic configuration of the Co atoms in the structure.[10b, 22] The pre-peak region of the TFY and TEY spectra can be deconvoluted with 3 gaussians, one assigned to the t_{2g} (octahedral and square-planar geometries) and two to the e_g $3z^2$ and x^2-y^2 orbital electron holes.[23] The presence of more than two peaks, confirms the complex nature of the Co spin states, thus not only present in low-spin configuration.[24] As observed by Karvonen et al.[25], throughout the series, the first pre-peak feature (~527 eV) more prominently present in the TFY than in the TEY data suggests a higher number of Co in octahedral geometry in the particles bulk than at the surface.

Focussing first in the TFY data, more representative of the bulk electronic structure, we observe two clear maxima in the pre-peak region for all samples. However, the complex nature of the Co atoms (i.e. the high number of parameters) does not allow for accurate deconvolution of the orbitals occupancies. The best estimation of the e_g/t_{g2} hole ratio was obtained by fitting the pre-peak regions with two Gaussians (t_{2g} and e_g respectively) in order to qualitatively compare the spectroscopic and magnetisation data, as discussed below.

Contrarily to XAS, which probes the unoccupied states in the *3d* levels, magnetization provides information on the number of unpaired Co *3d* electrons from the bulk structure. The Co electronic configuration of the different PBCO samples was investigated using SQUID magnetometry, which provides information on the bulk magnetic moment that can be used to estimate the average orbital occupation of the Co atoms. Figure 4 and Figure S6 (Supporting Information) show the temperature dependence of the molar magnetization and the inverse molar magnetic susceptibility (H/M) of the different PBCO samples, measured in a magnetic field of 0.1 T between 2 and 700 K. All five samples undergoes several magnetic transitions in this temperature range, as described in the literature for PBCO and in other layered Co perovskites.[10, 14, 26] In particular, the highest temperature transition, clearly seen in the H/M graph (Figure 4), has been interpreted as arising from a change of the Co spin state (Figure S7, Supporting Information). Since the OER measurements were performed at room temperature (RT), the effective paramagnetic moment per formula unit (μ_{eff}) of the different samples was calculated by fitting the temperature dependence of the inverse molar susceptibility with a Curie-Weiss law between 250 K and the spin-state transition at 350 K (Figure 4). The μ_{eff} values extracted from the obtained Curie constants are listed in Table S3, Supporting Information. These values, which agree well with literature data for the compounds where magnetization data have been reported, [26a, 26c, 26d, 27] reveal a decrease of μ_{eff} with the number of oxygen vacancies. This observation suggests that lower spin-states, which generally involve lower e_g occupations, are favored for the most O-deficient PBCO samples. Note that this happens in spite of the net increase of Co *3d* electrons expected from the evolution of the formal Co oxidation state from +3.30 (δ = 0.8) to +2.93 (δ = 0.43). To estimate the number of Co e_g electrons from the μ_{eff} values, it is important to realise that, in our samples, the Co atoms display different amounts of three different oxidation states (Co^{2+}, Co^{3+} and Co^{4+}) and two different coordination geometries (octahedral and square-pyramidal) with different CEF splitting (Δ_{CEF}). It is also important to remember that the 3d orbital occupation of Co is temperature dependent, as described earlier in the text. An illustrative example is provided by the sudden slope change on the inverse susceptibility of the δ = 0.43 and 0.48 PBCO samples at 350 K, attributed to a low-spin (LS, t_{2g}^6 eg^0 ,T < 350 K) to high-spin (HS, t_{2g}^4 eg^2, T > 350 K) transition of the Co^{3+} atoms in octahedral coordination.[26d] In order to identify the Co electronic configuration(s) compatible with the experimental μ_{eff} values we calculated for every PBCO sample the spin-only μ_{eff} values for all the possible combinations. Since several of them provided μ_{eff} values reasonably close to the experimental ones, only those satisfying well established physico-chemical criteria (such as the preference of higher oxidation states for higher coordinations) were retained (refer to the Table S3 caption for a detailed description of the theoretical considerations adopted).

10.1002/anie.202103151

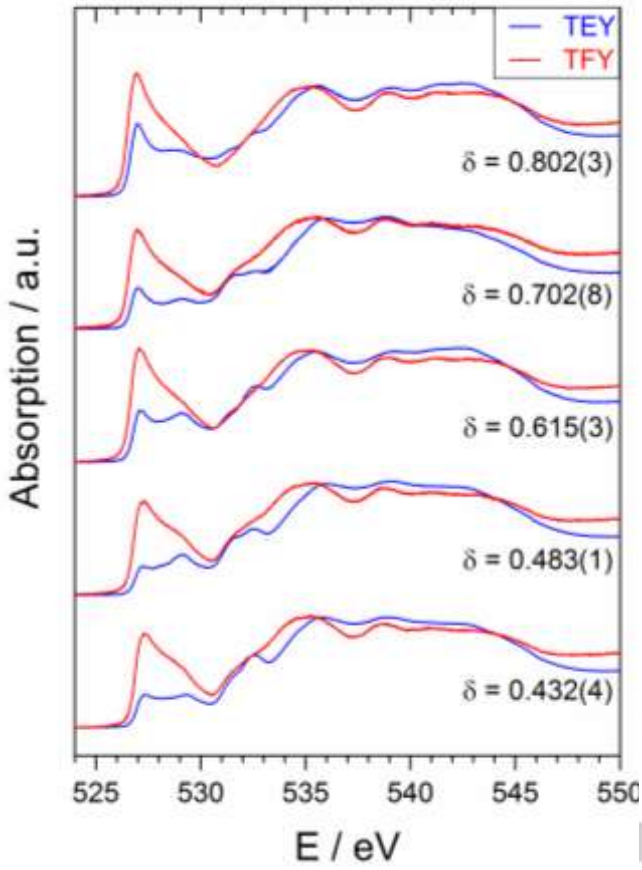

Figure 3. Pre-edge details of the PBCO O K-edge XAS data collected in total electron (TEY) and total fluorescence yield (TFY).

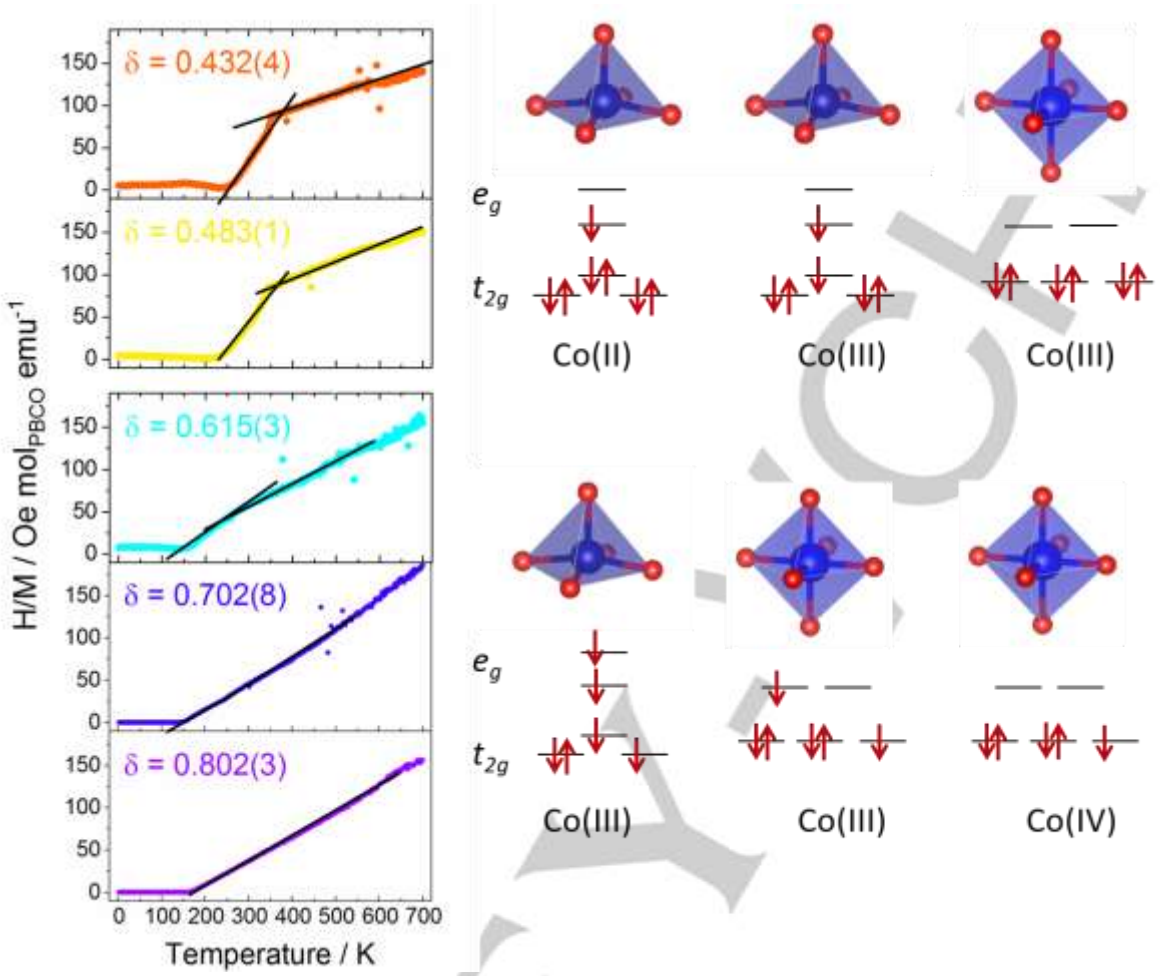

Figure 4. Temperature dependence of the PBCO inverse magnetic susceptibility (H/M) measured under a magnetic field of 0.1 T upon heating from 2 to 700 K. On the right, schematics of the Co atoms electronic configurations in the samples with δ < 0.5 and δ > 0.5 are shown. For a detailed description of the calculations, see Table S3 in the supplementary information file.

The resulting coordination and spin-state of Co^{2+}, Co^{3+} and Co^{4+} obtained for every PBCO sample are summarized in Figure 4, but given the complexity of the problem and the lack of a clear unique solution, they should be considered with caution. The resulting average e_g occupancies/Co atom for every sample are listed in Table S3, Supporting Information. As initially suggested by the μ_{eff} decrease upon oxygen removal, the average e_g occupation is progressively reduced from ≈ 2 to 1.07 by increasing the number of O vacancies. Both XAS and magnetisation data thus suggest that the electrons added by reducing the O content prefers to occupy the half-filled Co 3d orbitals instead of filling those being empty.

We now focus on the TEY pre-peak region of the O K-edge XAS spectra, more representative of the surface electronic structure and showed in Figure 3. In all the PBCO samples, the intensity of the TEY pre-peak region is substantially lower than in the TFY spectra. Moreover, the shape and intensity of the different features are markedly different, indicating a modification of the Co CEF levels and their occupations. Considering the relation between pre-peak area and the degree of the Co 3d-O 2p covalency,[25] these observations strongly suggest the existence of a structural reconstruction in the particle surface involving a decrease in the Co 3d – O 2p overlap. This aspect will be discussed in details in the next section where the aberration-corrected STEM images, with real space atomic resolution, are presented.

Catalyst surface characterization

Being the electrochemical water splitting a surface reaction, the difference between the TFY and TEY XAS at the O K-edge is an extremely interesting result that calls for further investigation of the catalyst surface region. Hence, understanding of the most active region of the catalyst and the differences with the easily analytically accessible bulk properties could shed light on the complex OER mechanism and thus on the key properties of the most OER active catalyst. To reach this goal, high-resolution STEM in combination with Electron Energy Loss Spectroscopy (EELS) provided a detailed picture of the unique structure, chemistry and electronic structure of the particles surface. When acquired in the high-angle annular dark-field (HAADF) imaging mode, the STEM images show the so-called Z-contrast, where the intensity of the atomic columns scales with the atomic number.[28] Figure 5 shows an atomic resolution Z-contrast image of the surface of the most active sample among the investigated series, δ = 0.43, in the *ab* plane, in which the brightest atomic columns correspond to the Ba and Pr atoms and the dimmer to the Co ones. Interestingly, this image also clearly shows the presence of a superstructure, visible with the contrast variations occurring every other Co-O plane (see orange lines). The image shows two different superstructure domains, perpendicular to each other. This well-known contrast stems from the structural

10.1002/anie.202103151

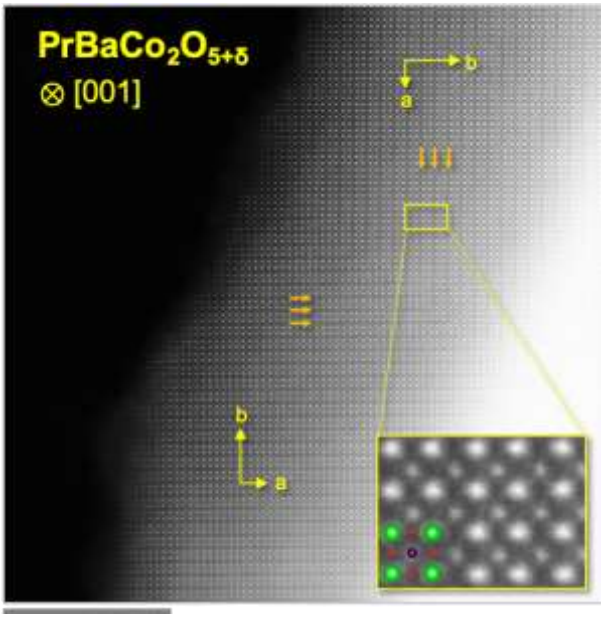

Figure 5. High-resolution HAADF (Z-contrast) image of the surface of the sample δ = 0.43 viewed along the [001] crystallographic axis. The vertical and horizontal dark stripes stem from the ordering of oxygen vacancies in every other Co-O plane. The inset shows a zoomed in region of the Z-contrast image with a superimposed perovskite schematic. Ba/Pr atoms in green, Co in blue and O in red.

relaxations resulting from the oxygen vacancies ordering in this PBCO phase. It is worth noting that this dark/bright pattern of Co-O planes appears as a result of a modulation in the cation spacing and the doubling of the $b = 2a_p$ parameter that results from the oxygen vacancy order, in good agreement with the conclusions inferred from bulk diffraction techniques. The HAADF images of the remaining samples, shown in Figure S15 in the Supporting Information, confirm the progressive decrease of oxygen vacancy order on oxygen increase, as described by the Rietveld refinements.

Concerning the surface, the first experimental evidence confirming the suspected partial modification with respect to the bulk came from the elemental-composition maps. Figure S10 shows the elemental map for the region close to the surface of a $PrBaCo_2O_{5.432}$ (δ = 0.43) particle. As the structure is viewed along the $[001]_{PBCO}$ zone-axis, the intensity of the Ba atomic columns, which in this orientation share the atomic colums with Pr, wanes at the surface, indicating a lower Ba content at the surface of the PBCO particle. The barium segregation has already been reported in the literature for long and high-temperature annealing processes on Ba containing perovskites, and it is expected to take place in similar proportions on the surface of all the tested samples (all prepared via high a thermal treatment).[29]

Besides the Ba off-stoichiometry right at the surface of the particle, further evidence of a substantial structural reconstruction in this region came from the images obtained using annular bright field (ABF) imaging in STEM. ABF and HAADZ (Z-contrast) imaging modes can be used simultaneously, which allows for the imaging and identification of all ions, including O columns, of the surface of the PBCO particle, see Figure 6. The image was acquired along the [110] zone axis in order to visualize the O sublattice along the Co-O plane. The contrast-inverted ABF image shown in Figure 6(d) (and Figure S16 for a selection of the remaining samples) unveils a complex surface structure, yet it reveals important variations of the PBCO structure at the surface, as the outer unit cells present substantial distortions. In particular, in this direction the Co columns appear strongly shifted towards the surface. These distortions must profoundly alter the electronic structure of the PBCO at the surface, which can be observed from simultaneously acquired EEL spectra. Figure 7 compares the fine structure of the O K edge several unit cells far from the surface and within the particle (Figure S11). The most notable difference is the decrease in intensity of the pre-peak of the O K edge (around 527 eV) at the surface. This result is in excellent agreement with those obtained from XAS (also shown in Figure 7), which also revealed differences in the O K edge fine structure between the bulk and the surface of the particles.

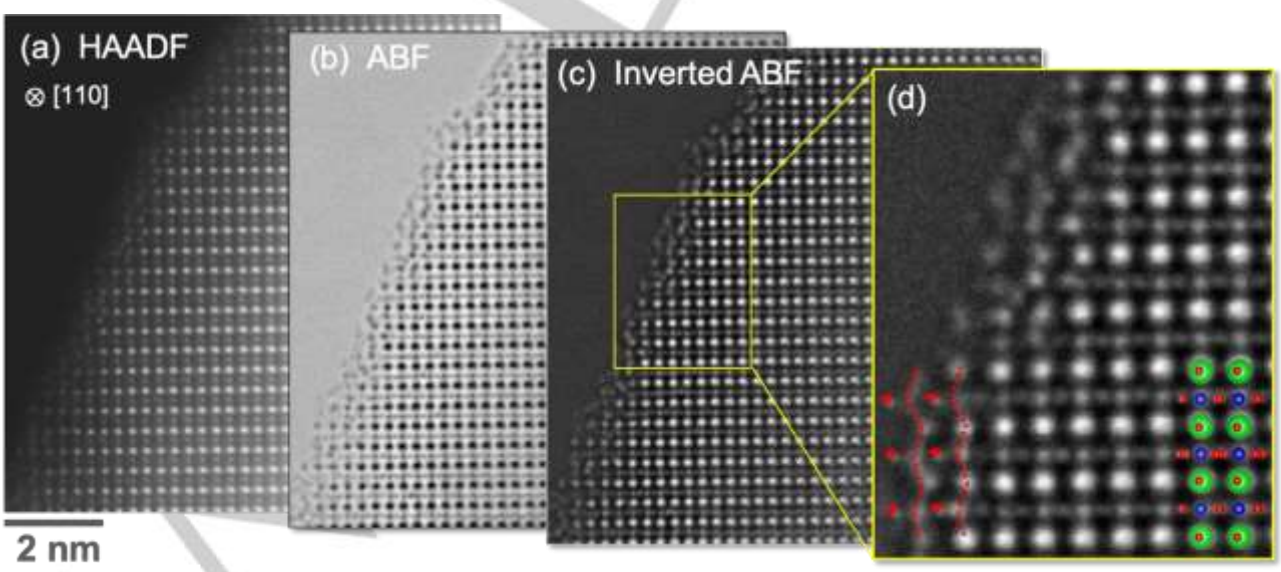

Figure 6.From left to right, (a) shows a high-resolution Z-contrast image of a PBCO particle with δ = 0.432 viewed along the [110]-zone axis, (b) the simultaneously acquired ABF image, (c) the inverted ABF image and (d) a zoomed in region of the surface from (c), along with the schematic structure viewed along this crystallographic axis. The dashed red lines connect different Ba/Pr cations with the off-centred Co columns, highlighting some of the distorted unit cells present at the surface.

10.1002/anie.202103151

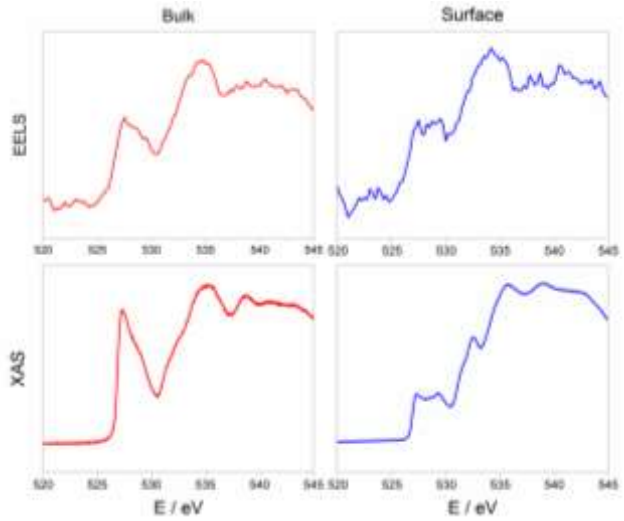

Figure 7. Comparison between the pre-peak region of the O K-edge bulk and surface spectra of sample δ = 0.432. On the top line: EELS spectra; on the bottom line: XAS TF and TEY data. All spectra are normalised with respect to the central peak intensity,

The different oxygen K-edge pre-peak features observed in the surface layer could originate from a rearrangement of the bulk crystal structure. As shown by the Z-contrast image in Figure 6, the Co atoms appear off-centred close to the particle surface, more precisely in the last two unit cells, where the Ba and most probably also the oxygen content are strongly depleted but the structural scaffold is maintained. The distorted structure would lead to fewer and less efficient Co 3d – O 2p overlap and hence a reduced area in the O K-edge pre-peak region. The presence of a distorted layer in the PBCO perovskite particles would explain both the Co displacements in the STEM images and the depletion of the O K-edge pre-peak observed in the XAS and EELS spectra by approaching the particle's surface.

To summarise, the STEM analysis clearly shows the different bulk and surface structural arrangement, with increasing distortion of the bulk perovskite structure approaching the particles surface. This involves a modified oxygen arrangement (as seen in the EELS and XAS depth-profile analysis) and the barium depletion on the particles surface.

Electrochemical characterisation. The five PBCO samples were tested for the OER activity in a three-electrode cell configuration, as detailed in the experimental section. Initially, a series of cyclic voltammetry measurements (see Figure S12, Supporting Information) were performed to stabilise the samples. Indeed, as shown in Figure S12, the samples show the largest drop in the OER current in the first 14th cycles, reaching a total loss of ~45% the initial value (considered to be the current density reached at the 2nd cycle). This result is in line with previous observations on PBCO nanoparticle catalysts,[9c] where the decrease of the PBCO OER activity upon stability cycles has been associated to a chemical cation dissolution process as anticipated by its Pourbaix diagram.[9c]

The Tafel plot of the PBCO series is shown in S13. All the samples present a similar slope of ~0.1 V dec^{-1}, suggesting that the same OER mechanism takes place on the surface of all the samples. The impact of the lattice oxygen vacancies in the water oxidation reaction is though evident when comparing the OER activity of the different samples at a fixed potential (chosen to be 1.65 V_{RHE}), reported in Figure 8.

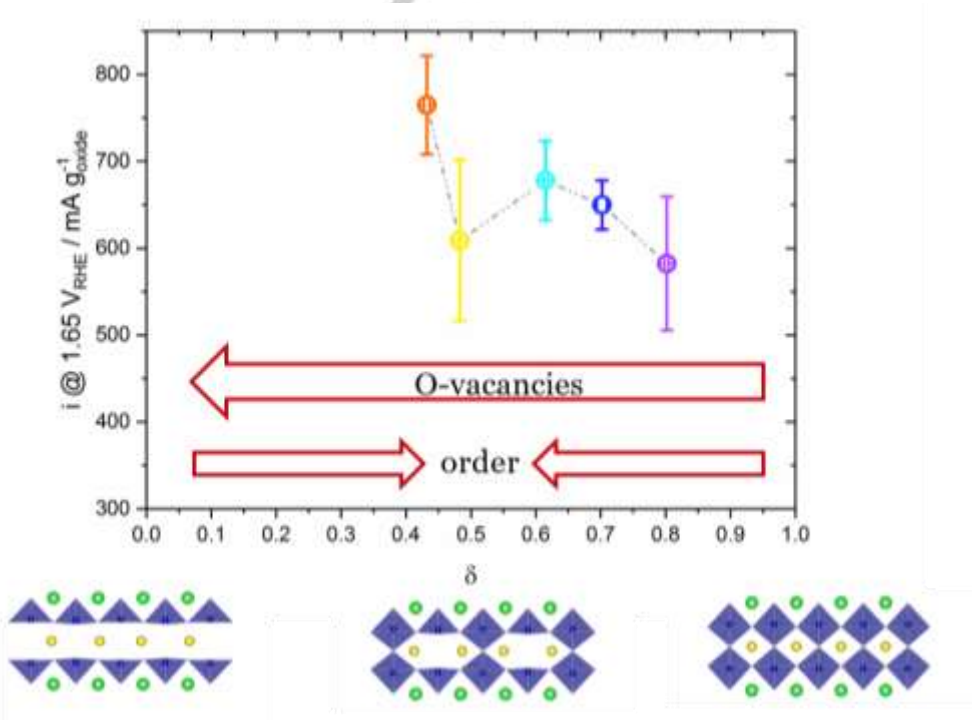

Figure 8. OER activity variation as function of oxygen stoichiometry in the $PrBaCo_2O_{5+\delta}$ samples. The oxygen vacancies distribution in the ordered PBCO structures with δ = 0, 0.5 and 1 are depicted at the bottom

.

It is important to note that the electrochemical activities are expressed in this work only as gravimetric current densities at 1.65 V_{RHE}. In fact, in order to obtain the proper data quality for the detailed diffraction refinements, highly crystalline materials are needed. These are obtained through long, high-temperature solid-state synthesis and annealing steps, which lead to big particles, in the range of hundreds of micrometres. The surface area of the PBCO samples used in this work is too small to be accurately measured by BET instruments[30] and therefore it was not used. The surface area were nevertheless evaluated, as a matter of comparison, obtaining similar values for the five samples (0.3 m^2 g^{-1} on average), as expected by the similar synthesis procedure and annealing temperatures, and in good agreement with previously reported BET surface area of PBCO samples prepared with similar synthesis routes (0.35 m^2 g^{-1}).[21c]

OER correlations

The OER activity of the PBCO samples mostly increases with the number of oxygen vacancies, with a visible drop for the sample with δ = 0.48 (see Figure 8).Overall the results clearly show that the initial lattice-oxygen content of the perovskite structure does affect the OER activity.[31] This suggests that the lattice oxygen evolution reaction (LOER), besides the conventional OER mechanism, takes place on the surface of the PBCO samples.[4, 7c-f] The participation of perovskite lattice oxygen to the OER generally leads to the catalyst surface reconstruction, specifically to the formation of a superficial oxyhydroxide layer.[5a, 6, 7b, 7e, 32] Furthermore, the LOER and the formation of the oxyhydroxide layer are also accompanied by cation dissolution as expressed in Equ. 1.

$$2ABO_{3-\delta} + 2OH^- \leftrightarrow 2BO(OH) + 2A_{aq}^{2+} + O_2(2-\delta) + 6e^- \quad (1)$$

The formation of a superficial oxyhydroxide layer does not necessarily leads to catalyst instability under OER conditions. Indeed, recent results suggest that for some OER catalysts a dynamic equilibrium between cation dissolution and re-deposition can be reached, leading to a co-existence of the perovskite structure and the superficial oxyhydroxide phase.[103,107–110,112,113] Furthermore, the self-assembled oxyhydroxide layer can itself undergo LOER and metal cation dissolution, as described in ref. [33]. Interestingly, it has been reported that the perovskite structure is not only “a precursor” for the active oxyhydroxide phase, but its presence underneath the active phase is necessary for high OER activity.[32a, 34] Vonrüti and Aschauer, using DFT, suggest that metastable materials under OER conditions can display the best OER activity due to the greatest diversity of reaction sites on the surface. Furthermore, samples with a large oxygen-vacancy content reasonably possess also a highly defective surface, where the oxyhydroxide reconstruction can easily take place. However, our data seems to suggest that not only the oxygen content, but also the local oxygen arrangement in the perovskite lattice strongly influence the OER activity. An important deviation from the general trend is in fact present at δ = 0.48, where the order of the oxygen vacancies is maximum in the crystal structure. Sharp physical properties modifications (for instance oxygen diffusion, spin state, resistivity) in the $RBaCo_2O_{5+\delta}$ series with δ ≈ 0.5 (so for sample δ = 0.48) have been extensively reported in the literature.[12, 35] In a recent publication,[36] the authors report a similar decrease in the OER activity for PBCO with δ ≈ 0.5, suggesting that the lower hybridisation of the Co 3d – O 2p orbitals reduces the charge transfer and thus the lattice oxygen redox activity.[21b, 37] The continuous reduction of the Co and O orbital hybridisation (proportional to the O-Co-O tilt in Figure S3, Supporting Information) on δ decrease however, does not explain the highest OER activity of the δ = 0.43 composition. Therefore, we do suggest that not only the oxygen content, but also its distribution (i.e., ordering) have an impact on the OER activity of perovskite structures. Oxygen vacancy ordering can influence the oxygen ion diffusivity within the perovskite structures, as shown for different composition[38] including PBCO.[39] The PBCO composition with the δ = 0.48 presents the highest oxygen vacancy order among the investigated series of samples. This suggests that the drop in OER activity at δ = 0.48 is due to oxygen vacancy order, which in turns reduces the oxygen diffusivity. In other words, the present result suggests that OER activity is influenced not only by the oxygen vacancy content, but also by the oxygen diffusivity in line with other recent studies on different perovskite materials.[7c-f]

Despite the beauty of finding a single perovskite properties governing the (L)OER activity, by varying the perovskite oxygen content many physico-chemical properties can be modified at the same time such as the crystal structure, cation ordering, electrical conductivity, electronic structure, etc. This obviously makes very difficult identifying the so called “perovskite activity descriptors”. In the present study, by studying perovskite catalysts with same cation composition and morphology but different oxygen content, the perovskite physico-chemical properties that can affect the OER have been minimized. However, to better exclude that the OER activity differences observed in the PBCO series are only due to oxygen vacancy content and ordering, the possible contribution of other measureable PBCO physico-chemical properties on the OER activity has been examined. Figure 9 shows that no clear correlation was found between the OER activity and several activity descriptors. The OER activity does not follow the electronic conductivity measured for the powder samples (Figure S14, Supporting Information), which increases with the oxygen content of the samples, nor the Co 3d – O 2p orbitals hybridisation.

10.1002/anie.202103151

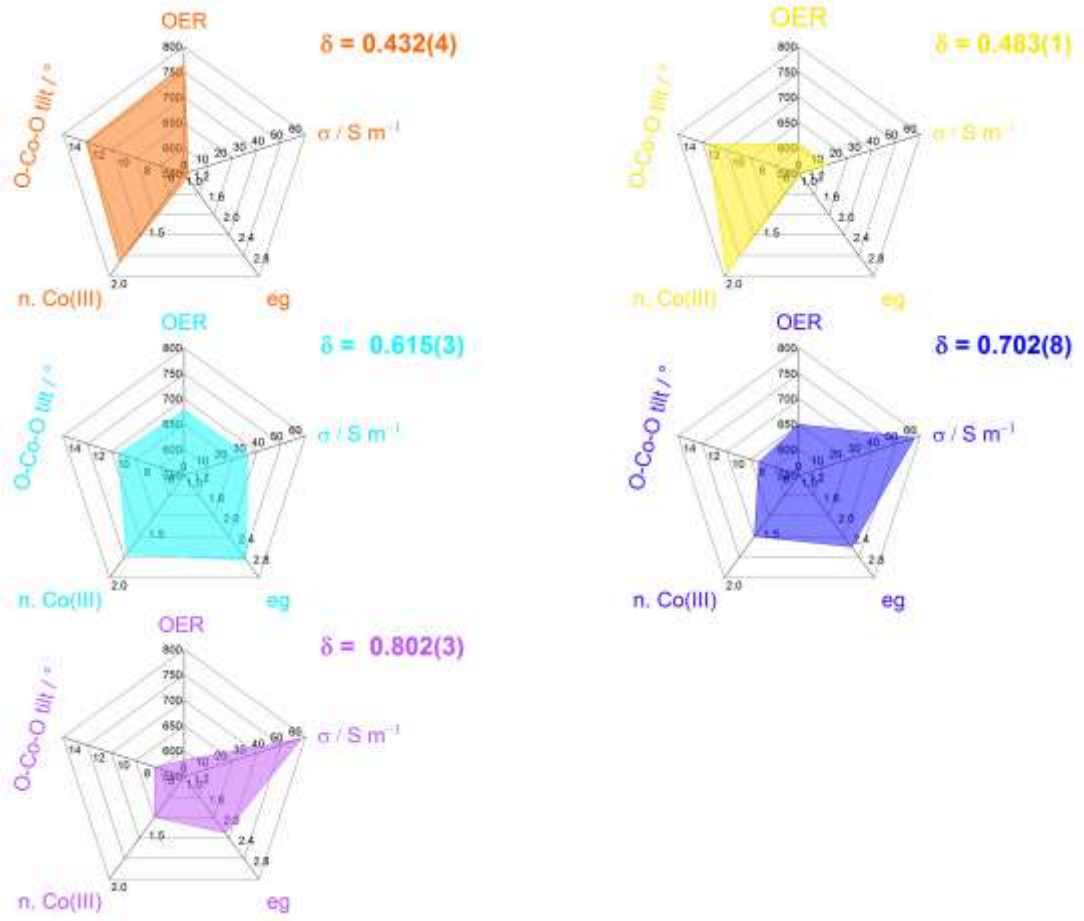

Figure 9. Summary of the main parameters considered in this work as activity descriptors.

Conclusion

The systematic study of the correlation between oxygen The systematic study of the correlation between oxygen stoichiometry and OER activity in the $PrBaCo_2O_{5+\delta}$ materials shows an increase of the activity upon lattice oxygen vacancies increase. Being postulated that the oxygen vacancies take part to the reaction mechanism involving the oxidation of the lattice oxygen, the LOER, this study provides a contribution to the understanding of the key parameters affecting the OER activity and further validates the occurrence of LOER on highly active perovskite catalysts. Furthermore, the trend of OER activity *vs*. oxygen vacancies content in not linear, indicating that other aspects should be considered to fully understand the OER mechanism on perovskites samples. A clear activity drop is present for $\delta \sim 0.5$, where the oxygen-vacancies in the Pr plane order forming alternating [CoO_6] octahedral and [CoO_5] square pyramids, with clear changes in the Co-O coordination and O-Co-O plane buckling. This suggests that oxygen vacancy ordering is detrimental for the OER activity of perovskites. The OER activity was compared also with other physicochemical properties of the perovskite material, such as electronic conductivity, Co 3d – O 2p orbitals hybridisation and electronic configuration but in none of them a clear correlation was observed. However, our detailed sample characterization also revealed the complexity of these materials and the macroscopic inaccuracies caused by the approximation in the data analysis or properties assumptions (clear in the electronic structure analysis).

The O K-edge XAS data and the STEM images shows the differences between particle bulk and surface, even in the pristine catalyst. The comprehensive study of the particle surface, which is the region involved in the electrochemical OER process, is still particularly complex and limited, but it could provide additional information on the key parameters affecting the OER activity and on the reaction mechanism. This highlights the need for operando, surface-sensitive techniques

Acknowledgements

The X-ray absorption measurements were performed on the EPFL/PSI X-Treme beamline (O K-edge) and at the SuperXAS beamline (Co K-edge) at the Swiss Light Source, Paul Scherrer Institute, Villigen, Switzerland. The diffraction measurements were performed at the HRPT instrument at the Swiss spallation neutron source SINQ and at the MS-beamline at the Swiss Light Source at the Paul Scherrer Institute. The authors acknowledge the MS team for the measurements (Mesquik proposal 20182326). JG acknowledges Ramón y Cajal contract RYC-2012-11709 and the Severo Ochoa SEV-2015-0496 Project. The authors acknowledge the ICTS-CNME at UCM for offering access to their instruments and expertise and the Paul Scherrer Institute, for financial support through the internal CROSS project. TJS thanks Innosuisse and the Swiss Competence Centre for Energy Research (SCCER) Heat & Electricity Storage.

Keywords: water splitting • electrolyzers • perovskite • lattice oxygen evolution reaction • activity descriptor

References

[1] E. Fabbri, A. Habereder, K. Waltar, R. Kötz, T. J. Schmidt, *Catalysis Science & Technology* **2014**, *4*, 3800-3821.

[2] aJ. Suntivich, K. J. May, H. A. Gasteiger, J. B. Goodenough, Y. Shao-Horn, *Science* **2011**, *334*, 1383-1385; bS. Trasatti, *Journal of Electroanalytical Chemistry* **1980**, *111*, 125-131.

[3] aW. T. Hong, M. Risch, K. A. Stoerzinger, A. Grimaud, J. Suntivich, Y. Shao-Horn, *Energy & Environmental Science* **2015**, *8*, 1404-1427; bJ. Hwang, R. R. Rao, L. Giordano, Y. Katayama, Y. Yu, Y. Shao-Horn, *Science* **2017**, *358*, 751-756.

[4] T. Binninger, R. Mohamed, K. Waltar, E. Fabbri, P. Levecque, R. Kötz, T. J. Schmidt, *Scientific Reports* **2015**, *5*, 12167.

[5] aE. Fabbri, M. Nachtegaal, T. Binninger, X. Cheng, B.-J. Kim, J. Durst, F. Bozza, T. Graule, R. Schäublin, L. Wiles, M. Pertoso, N. Danilovic, K. E. Ayers, T. J. Schmidt, *Nature Materials* **2017**, *16*, 925-931; bH. M. A. Amin, P. Königshoven, M. Hegemann, H. Baltruschat, *Analytical Chemistry* **2019**, *91*, 12653-12660.

[6] E. Fabbri, T. J. Schmidt, *ACS Catalysis* **2018**, *8*, 9765-9774.

[7] aE. Fabbri, M. Nachtegaal, X. Cheng, T. Binninger, B. Kim, J. Durst, F. Bozza, T. Graule, N. Danilocic, K. E. Ayers, T. J. Schmidt, *Nature Materials* **2017**, *16*, 925–931 ; bB.-J. Kim, E. Fabbri, D. F. Abbott, X. Cheng, A. H. Clark, M. Nachtegaal, M. Borlaf, I. E. Castelli, T. Graule, T. J. Schmidt, *Journal of the American Chemical Society* **2019**, *141*, 5231-5240; cR. P. Forslund, W. G. Hardin, X. Rong, A. M. Abakumov, D. Filimonov, C. T. Alexander, J. T. Mefford, H. Iyer, A. M. Kolpak, K. P. Johnston, K. J. Stevenson, *Nature communications* **2018**, *9*, 3150; dJ. T. Mefford, X. Rong, A. M. Abakumov, W. G. Hardin, S. Dai, A. M. Kolpak, K. P. Johnston, K. J. Stevenson, *Nature Communications* **2016**, *7*, 11053; eY. Pan, X. Xu, Y. Zhong, L. Ge, Y. Chen, J.-P. M. Veder, D. Guan, R. O'Hayre, M. Li, G. Wang, H. Wang, W. Zhou, Z. Shao, *Nature Communications* **2020**, *11*, 2002; fY. Zhu, Q. Lin, Z. Hu, Y. Chen, Y. Yin, H. A. Tahini, H.-J. Lin, C.-T. Chen, X. Zhang, Z. Shao, H. Wang, **2020**, *16*, 2001204; gN.-I. Kim, Y. J. Sa, T. S. Yoo, S. R. Choi, R. A. Afzal, T. Choi, Y.-S. Seo, K.-S. Lee, J. Y. Hwang, W. S. Choi, S. H. Joo, J.-Y. Park, *Science Advances* **2018**, *4*.

[8] X. Cheng, E. Fabbri, Y. Yamashita, I. E. Castelli, B. Kim, M. Uchida, R. Haumont, I. Puente-Orench, T. J. Schmidt, *ACS Catalysis* **2018**, *8*, 9567-9578.

[9] aA. Grimaud, K. J. May, C. E. Carlton, Y. L. Lee, M. Risch, W. T. Hong, J. G. Zhou, Y. Shao-Horn, *Nature Communications* **2013**, *4*; bB.-J. Kim, E. Fabbri, I. E. Castelli, M. Borlaf, T. Graule, M. Nachtegaal, T. J. Schmidt, **2019**, *9*, 263; cB.-J. Kim, X. Cheng, D. F. Abbott, E. Fabbri, F. Bozza, T. Graule, I. E. Castelli, L. Wiles, N. Danilovic, K. E. Ayers, N. Marzari, T. J. Schmidt, *Advanced Functional Materials* **2018**, *28*, 1804355.

[10] aS. Streule, A. Podlesnyak, J. Mesot, M. Medarde, K. Conder, E. Pomjakushina, E. Mitberg, V. Kozhevnikov, *Journal of Physics: Condensed Matter* **2005**, *17*, 3317-3324; bX. Zhang, X.-M. Wang, H.-W. Wei, X.-H. Lin, C.-H. Wang, Y. Zhang, C. Chen, X.-P. Jing, *Materials Research Bulletin* **2015**, *65*, 80-88; cC. Frontera, A. Caneiro, A. E. Carrillo, J. Oró-Solé, J. L. García-Muñoz, *Chemistry of Materials* **2005**, *17*, 5439-5445.

[11] B.-J. Kim, E. Fabbri, M. Borlaf, I. E. Castelli, M. Nachtegaal, T. Graule, T. J. Schmidt, *submitted* **2020**.

[12] A. A. Taskin, A. N. Lavrov, Y. Ando, *Physical Review B* **2005**, *71*, 134414.

[13] K. Conder, E. Pomjakushina, A. Soldatov, E. Mitberg, *Materials Research Bulletin* **2005**, *40*, 257-263.

[14] M. M. Seikh, V. Pralong, O. I. Lebedev, V. Caignaert, B. Raveau, *Journal of Applied Physics* **2013**, *114*, 013902.

[15] R. Shannon, *Acta Crystallographica Section A* **1976**, *32*, 751-767.

[16] W. A. Harrison, *Electronic Structure and the Properties of Solids: The Physics of the Chemical Bond*, Dover Publications, **2012**.

[17] M. Medarde, J. Mesot, P. Lacorre, S. Rosenkranz, P. Fischer, K. Gobrecht, *Physical Review B* **1995**, *52*, 9248-9258.

[18] M. Medarde, C. Dallera, M. Grioni, B. Delley, F. Vernay, J. Mesot, M. Sikora, J. A. Alonso, M. J. Martínez-Lope, *Physical Review B* **2009**, *80*, 245105.

[19] B.-J. Kim, E. Fabbri, I. E. Castelli, M. Borlaf, T. Graule, M. Nachtegaal, T. J. Schmidt, *Catalysts* **2019**, *9*, 263.

[20] M. Medarde, C. Dallera, M. Grioni, J. Voigt, A. Podlesnyak, E. Pomjakushina, K. Conder, T. Neisius, O. Tjernberg, S. N. Barilo, *Physical Review B* **2006**, *73*, 054424.

[21] aJ. Suntivich, H. A. Gasteiger, N. Yabuuchi, H. Nakanishi, J. B. Goodenough, Y. Shao-Horn, *Nature Chemistry* **2011**, *3*, 546-550; bJ. T. Mefford, X. Rong, A. M. Abakumov, W. G. Hardin, S. Dai, A. M. Kolpak, K. P. Johnston, K. J. Stevenson, *Nature Communications* **2016**, *7*, 11053; cA. Grimaud, K. J. May, C. E. Carlton, Y.-L. Lee, M. Risch, W. T. Hong, J. Zhou, Y. Shao-Horn, *Nature Communications* **2013**, *4*, 2439.

[22] aY. Orikasa, T. Ina, T. Nakao, A. Mineshige, K. Amezawa, M. Oishi, H. Arai, Z. Ogumi, Y. Uchimoto, *The Journal of Physical Chemistry C* **2011**, *115*, 16433-16438; bM. Abbate, J. C. Fuggle, A. Fujimori, L. H. Tjeng, C. T. Chen, R. Potze, G. A. Sawatzky, H. Eisaki, S. Uchida, *Physical Review B* **1993**, *47*, 16124-16130.

[23] aP. M. Woodward, P. Karen, *Inorganic Chemistry* **2003**, *42*, 1121-1129; bZ. Hu, H. Wu, M. W. Haverkort, H. H. Hsieh, H. J. Lin, T. Lorenz, J. Baier, A. Reichl, I. Bonn, C. Felser, A. Tanaka, C. T. Chen, L. H. Tjeng, *Physical Review Letters* **2004**, *92*, 207402.

[24] F. M. F. de Groot, M. Grioni, J. C. Fuggle, J. Ghijsen, G. A. Sawatzky, H. Petersen, *Physical Review B* **1989**, *40*, 5715-5723.

[25] L. Karvonen, M. Valkeapää, R.-S. Liu, J.-M. Chen, H. Yamauchi, M. Karppinen, *Chemistry of Materials* **2010**, *22*, 70-76.

[26] aS. Ganorkar, K. R. Priolkar, P. R. Sarode, A. Banerjee, R. Rawat, S. Emura, *Journal of Physics: Condensed Matter* **2012**, *24*, 476003; bS. Ganorkar, K. R. Priolkar, P. R. Sarode, A. Banerjee, *Journal of Applied Physics* **2011**, *110*, 053923; cC. Frontera, J. L. García-Muñoz, A. E. Carrillo, C. Ritter, D. Martín y Marero, A. Caneiro, *Physical Review B* **2004**, *70*, 184428; dC. Frontera, J. L. García-Muñoz, A. E. Carrillo, M. A. G. Aranda, I. Margiolaki, A. Caneiro, *Physical Review B* **2006**, *74*, 054406.

[27] C. Frontera, J. L. García-Muñoz, A. E. Carrillo, A. Caneiro, C. Ritter, D. M. y. Marero, *Journal of Applied Physics* **2005**, *97*, 10C106.

[28] S. J. Pennycook, D. E. Jesson, *Ultramicroscopy* **1991**, *37*, 14-38.

[29] B. Wei, M. Schroeder, M. Martin, *ACS Applied Materials & Interfaces* **2018**, *10*, 8621-8629.

[30] M. Thommes, K. Kaneko, V. Neimark Alexander, P. Olivier James, F. Rodriguez-Reinoso, J. Rouquerol, S. W. Sing Kenneth, in *Pure and Applied Chemistry, Vol. 87*, **2015**, p. 1051.

[31] aJ. Bao, X. Zhang, B. Fan, J. Zhang, M. Zhou, W. Yang, X. Hu, H. Wang, B. Pan, Y. Xie, *Angewandte Chemie International Edition* **2015**, *54*, 7399-7404; bN.-I. Kim, Y. J. Sa, T. S. Yoo, S. R. Choi, R. A. Afzal, T. Choi, Y.-S. Seo, K.-S. Lee, J. Y. Hwang, W. S. Choi, S. H. Joo, J.-Y. Park, *Science Advances* **2018**, *4*, eaap9360; cT. Ling, D.-Y. Yan, Y. Jiao, H. Wang, Y. Zheng, X. Zheng, J. Mao, X.-W.

Du, Z. Hu, M. Jaroniec, S.-Z. Qiao, *Nature Communications* **2016**, *7*, 12876.

[32] aP. P. Lopes, D. Y. Chung, X. Rui, H. Zheng, H. He, P. Farinazzo Bergamo Dias Martins, D. Strmcnik, V. R. Stamenkovic, P. Zapol, J. F. Mitchell, R. F. Klie, N. M. Markovic, *Journal of the American Chemical Society* **2021**; bD. Y. Chung, P. P. Lopes, P. Farinazzo Bergamo Dias Martins, H. He, T. Kawaguchi, P. Zapol, H. You, D. Tripkovic, D. Strmcnik, Y. Zhu, S. Seifert, S. Lee, V. R. Stamenkovic, N. M. Markovic, *Nature Energy* **2020**, *5*, 222-230; cT. Wu, S. Sun, J. Song, S. Xi, Y. Du, B. Chen, W. A. Sasangka, H. Liao, C. L. Gan, G. G. Scherer, L. Zeng, H. Wang, H. Li, A. Grimaud, Z. J. Xu, *Nature Catalysis* **2019**, *2*, 763-772; dC. Zhao, N. Li, R. Zhang, Z. Zhu, J. Lin, K. Zhang, C. Zhao, *ACS Applied Materials & Interfaces* **2019**, *11*, 47858-47867.

[33] T. Binninger, R. Mohamed, K. Waltar, E. Fabbri, P. Levecque, R. Kötz, T. J. Schmidt, *Scientific Reports* **2015**, *5*, 12167.

[34] X. Cheng, B.-J. Kim, E. Fabbri, T. J. Schmidt, *ACS Applied Materials & Interfaces* **2019**.

[35] aA. A. Taskin, A. N. Lavrov, Y. Ando, *Applied Physics Letters* **2005**, *86*, 091910; bS. Roy, I. S. Dubenko, M. Khan, E. M. Condon, J. Craig, N. Ali, W. Liu, B. S. Mitchell, *Physical Review B* **2005**, *71*, 024419; cH. D. Zhou, J. B. Goodenough, *Journal of Solid State Chemistry* **2004**, *177*, 3339-3345.

[36] X. Miao, L. Wu, Y. Lin, X. Yuan, J. Zhao, W. Yan, S. Zhou, L. Shi, *Chemical Communications* **2019**, *55*, 1442-1445.

[37] A. Grimaud, O. Diaz-Morales, B. Han, W. T. Hong, Y.-L. Lee, L. Giordano, K. A. Stoerzinger, M. T. M. Koper, Y. Shao-Horn, *Nature Chemistry* **2017**, *9*, 457-465.

[38] aS. Adler, S. Russek, J. Reimer, M. Fendorf, A. Stacy, Q. Huang, A. Santoro, J. Lynn, J. Baltisberger, U. Werner, *Solid State Ionics* **1994**, *68*, 193-211; bM. V. Patrakeev, I. A. Leonidov, E. B. Mitberg, A. A. Lakhtin, V. G. Vasiliev, V. L. Kozhevnikov, K. R. Poeppelmeier, *Ionics* **1999**, *5*, 444-449.

[39] B. Mace, Z. Harrell, X. Xu, C. Chen, E. Enriquez, A. Chen, Q. Jia, *Journal of Materiomics* **2018**, *4*, 51-55.

10.1002/anie.202103151

Entry for the Table of Contents

Insert graphic for Table of Contents here.

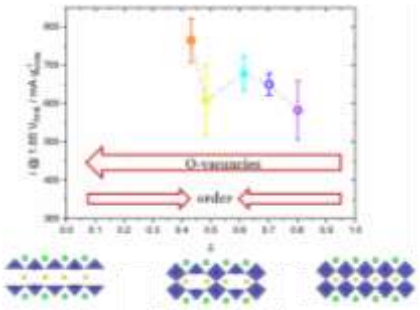

Oxygen vacancies content and ordering is influencing the oxygen evolution reaction activity of one of the most active perovskite electrocatalyst, PrBaCo2O5+d. It is suggested that a high oxygen vacancy content in the perovskite lattice is beneficial for the activity, while lattice oxygen ordering leads to a drop in the OER activity.